Advances in Applied Mathematics and Mechanics
Adv. Appl. Math. Mech., Vol. **9**, No. 1, pp. 125-143

DOI: 10.4208/aamm.2015.m1143
February 2017

XFEM for Fracture Analysis in 2D Anisotropic Elasticity

Honggang Jia[1,2], Yufeng Nie[2,*] and Junlin Li[3]

[1] *School of Mathematics and Statistics, Xuchang University, Xuchang, Henan 461000, China*
[2] *Department of Applied Mathematics, School of Science, Northwestern Polytechnical University, Xi'an, Shaanxi 710129, China*
[3] *School of Applied Science, Taiyuan University of Science and Technology, Taiyuan, Shanxi 030024, China*

Received 7 June 2015; Accepted (in revised version) 31 December 2015

Abstract. In this paper, a method is proposed for extracting fracture parameters in anisotropic thermoelasticity cracking via interaction integral method within the framework of extended finite element method (XFEM). The proposed method is applied to linear thermoelastic crack problems. The numerical results of the stress intensity factors (SIFs) are presented and compared with those reported in related references. The good agreement of the results obtained by the developed method with those obtained by other numerical solutions proves the applicability of the proposed approach and confirms its capability of efficiently extracting thermoelasticity fracture parameters in anisotropic materials.

AMS subject classifications: 65M60, 74A45

Key words: Anisotropic materials, thermoelasticity, crack, XFEM, stress intensity factors.

1 Introduction

Anisotropic materials, such as glass/epoxy, crystal, phenolic laminated sheet materials, etc., are widely used in many practical engineering structures due to their superior directional mechanical properties. During mechanical analysis and product design, it is generally necessary to consider anisotropic effects of the components produced from anisotropic materials. This has resulted in an upsurge of developing new fracture mechanical methods in anisotropic materials. The earliest paper about fracture problems in anisotropic materials was launched by Muskhelishvili [1]. Afterwards, G. C. Sih, P.

*Corresponding author.
Email: yfnie@nwpu.edu.cn (Y. F. Nie)

C. Paris and G. R. Irwin investigated the crack problems in rectilinearly anisotropic bodies [2]. Studies of Z. Suo [3]solved some problems in singularities and cracks in dissimilar anisotropic medium. L. Nobile et al. [4] proposed an analytical method to study fracture problems in anisotropic/orthotropic medium. S. G. Lekhnitskii [5] researched on the elastic theory in anisotropic materials. S. Q. Zhang et al. [6] predicted the growth of Mode I crack in fiber reinforced composite. H. G. Jia, Y. F. Nie [7] proposed a method for simulating orthotropic thermoelasticity fracture. However, all above-mentioned works can only solve crack problems with simple geometry configuration and load. In view of this, numerical methods such as finite element method (FEM) [8, 9], boundary element method (BEM) [10–13], meshless method [14–16], and extended finite element method (XFEM) [17–20] have been developed to study more complicated fracture mechanical problems concerning mechanical and/or thermal load in anisotropic medium. Especially, in fracture of thermoelasticity in anisotropic medium, Y. C. Shiah et al. [10,13] used BEM to analyze thermoelastic fracture in generally anisotropic materials. G. Hattori et al. [18] developed anisotropic crack-tip enrichment functions using Stroh's formalism within the framework of XFEM. S. S. Hosseini et al. [20] developed a new XFEM to analyze crack propagation in functionally graded materials. However, in these works, there is little attention paid to thermoelastic fracture analyzed by XFEM in fully anisotropic materials using anisotropic crack tip enrichment functions with Stroh's formalism.

In this paper, thermoelastic fracture analysis is performed via XFEM in fully anisotropic materials, and the SIFs around crack tips are obtained by domain formulation of interaction integral method combined with XFEM. On this basis, several numerical examples are given to validate the accuracy of results. To the best knowledge of the authors, it is the first time that applying XFEM with Stroh's formalism crack tip enrichment functions to fracture analysis of anisotropic composites under thermal loadings.

The rest of this paper is structured as follows. Fracture mechanics of anisotropic materials are given in Section 2. Section 3 states the governing equations of the problem and the discretization of the thermoelastic XFEM. Then, Section 4 gives the extraction of the SIFs from the XFEM by using domain formulation of interaction integrals with thermal effect. In Section 5, the proposed method is validated by several numerical examples and is compared with available solutions in literature. Finally, the conclusions from this research are summarized in Section 6.

2 Fracture mechanics of anisotropic materials

2.1 Constitutive relation of anisotropic materials

For anisotropic materials, the stress-strain relations [2] can be expressed as follows:

$$\varepsilon_i = \sum_{j=1}^{6} a_{ij}\sigma_j, \quad a_{ij} = a_{ji}, \quad (i = 1,2,6), \tag{2.1}$$

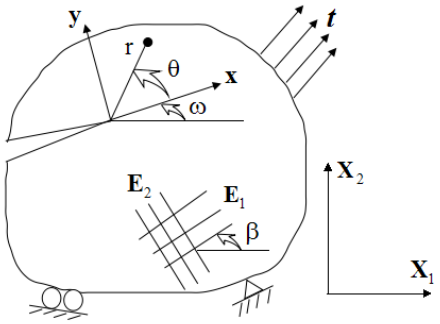

Figure 1: A generally anisotropic body subjected to traction t, with global Cartesian co-ordinate (X_1,X_2), local Cartesian co-ordinate (x,y) local crack tip polar co-ordinate (r,θ) and various boundary conditions.

with $\varepsilon_1=\varepsilon_{11}$, $\varepsilon_2=\varepsilon_{22}$, $\varepsilon_3=\varepsilon_{33}$, $\varepsilon_4=2\varepsilon_{23}$, $\varepsilon_5=2\varepsilon_{31}$, $\varepsilon_6=2\varepsilon_{12}$, $\sigma_1=\sigma_{11}$, $\sigma_2=\sigma_{22}$, $\sigma_3=\sigma_{33}$, $\sigma_4=\sigma_{23}$, $\sigma_5=\sigma_{31}$, $\sigma_6=\sigma_{12}$. Where a_{ij} is components of anisotropic compliance tensor. Here, a two-dimensional plane stress state is assumed. Fig. 1 shows a crack in the fully anisotropic body [21] subjected to arbitrary loading and boundary conditions,where (X_1,X_2) represents global Cartesian co-ordinate, (x,y) be local Cartesian co-ordinate and (r,θ) represents the local crack tip co-ordinate, and β is the angle between elastic principal direction and X_1-axis.

2.2 Asymptotic fields near the crack tip for anisotropic medium

The near-tip asymptotic displacement field in a plane anisotropic medium can be written in Stroh's formalism [3] as follows:

$$u_i(r,\theta)=\sqrt{\frac{2}{\pi}}Re\Big(K_\alpha A_{im}B_{m\alpha}^{-1}\sqrt{r(\cos\theta+\mu_m\sin\theta)}\Big), \tag{2.2}$$

where $i,m=1,2$, $\alpha=I,II$ is associated with the fracture modes of I, II, and denotes the real part. Here, the summation convention holds for over repeated indices.

Similarly, the near-tip asymptotic stress fields can be written as

$$\sigma_{ij}(r,\theta)=(-1)^j\sqrt{\frac{1}{2\pi}}Re\Big(K_\alpha B_{im}B_{m\alpha}^{-1}\frac{\delta_{j1}\mu_m+\delta_{j2}}{\sqrt{r(\cos\theta+\mu_m\sin\theta)}}\Big), \tag{2.3}$$

where δ_{jk}represents the Kronecker-delta.

In Eqs. (2.2) and (2.3), μ_m denote a distinct complex number with positive imaginary part. These two complex numbers can be obtained by solving the characteristic equation in anisotropic materials.

$$a_{11}\mu_m^4-2a_{16}\mu_m^3+(2a_{12}+a_{66})\mu_m^2-2a_{26}\mu_m+a_{22}=0. \tag{2.4}$$

The roots of Eq. (2.4) are always either complex or purely imaginary in conjugate pairs as μ_m, $\bar{\mu_m}$.

3 Governing equations of the problem and the discretization of the thermoelastic XFEM

3.1 Governing equations

For the 2D case, the static linear anisotropic thermoelasticity equations in a domain Ω bounded by Γ are

$$\mathbf{q}=-\mathbf{k}\nabla T\mathbf{k}=\begin{bmatrix} k_1 & 0 \\ 0 & k_2 \end{bmatrix}, \tag{3.1a}$$

$$-\mathbf{q}+\bar{Q}=-\mathbf{0}, \tag{3.1b}$$

$$\boldsymbol{\varepsilon}=\nabla_s\mathbf{u}, \tag{3.1c}$$

$$\boldsymbol{\varepsilon}_\mathbf{T}=\boldsymbol{\alpha}(T-T_0)\mathbf{I}\boldsymbol{\alpha}=\begin{bmatrix} \alpha_1 & 0 \\ 0 & \alpha_2 \end{bmatrix}, \tag{3.1d}$$

$$\boldsymbol{\varepsilon}_m=\boldsymbol{\varepsilon}-\boldsymbol{\varepsilon}_\mathbf{T}, \tag{3.1e}$$

$$\boldsymbol{\sigma}=\mathbf{C}:\boldsymbol{\varepsilon}_m, \tag{3.1f}$$

$$\nabla\cdot\boldsymbol{\sigma}+\bar{\mathbf{b}}=\mathbf{0}, \tag{3.1g}$$

where T is the temperature; T_0 is the reference temperature; $\mathbf{q}$ is the heat flux; k_1, k_2 are the diffusivities in x, y directions,respectively; α_1, α_2 are the expansion coefficients in x, y directions, respectively; $\mathbf{u}$ is the displacement; $\boldsymbol{\varepsilon}$ is the total strain tensor; $\boldsymbol{\varepsilon}_m$ is the mechanical strain tensor; $\boldsymbol{\varepsilon}_T$ is the thermal expansion stain; $\boldsymbol{\sigma}$ is the stress tensor; $\mathbf{C}$ is the anisotropic Hooke tensor; $\bar{Q}$ is the heat source; $\bar{\mathbf{b}}$ is the body force; $\mathbf{I}$ is the the identity tensor; and ∇_s is the symmetric gradient operator. The boundary conditions are as follows:

$$\mathbf{u}=\bar{\mathbf{u}} \quad \text{on } \Gamma_u, \tag{3.2a}$$

$$\boldsymbol{\sigma}\cdot\mathbf{n}=\bar{\mathbf{t}} \quad \text{on } \Gamma_t, \tag{3.2b}$$

$$\boldsymbol{\sigma}\cdot\mathbf{n}=\mathbf{0} \quad \text{on } \Gamma_c, \tag{3.2c}$$

$$T=\bar{T} \quad \text{on } \Gamma_T, \tag{3.2d}$$

$$\mathbf{q}\cdot n=\bar{\mathbf{q}} \quad \text{on } \Gamma_q. \tag{3.2e}$$

Here, $\Gamma_T\cup\Gamma_q=\Gamma_u\cup\Gamma_t=\Gamma$ and $\Gamma_T\cap\Gamma_q=\Gamma_u\cap\Gamma_t=\emptyset$ (empty set). Assuming an adiabatic crack Γ_c with null traction is present in Ω, then $\Gamma_c\subset\Gamma_t$, $\bar{\mathbf{t}}=\mathbf{0}$ on Γ_c and $\Gamma_c\subset\Gamma_q$, $\bar{q}=\mathbf{0}$ on Γ_c.

3.2 XFEM for anisotropic thermoelastic crack

3.2.1 XFEM for modeling anisotropic thermoelastic crack

The extended finite element method (XFEM) has been widely used for analysis of various fracture or fatigue problems. XFEM is an improved finite element method based on the

partition of unity method that is appropriately designed for the problems associated with discontinuity and singularity.

The isoparametric finite element shape function $N_k(x)$ satisfies the partition of unity property in Ω, i.e.,

$$\sum_{k=1}^{m} N_k(x) = 1, \quad x \in \Omega. \tag{3.3}$$

For an arbitrary function $f(x)$ in Ω, finite element shape function $N_k(x)$ in Eq. (3.3) also satisfies the reproducing condition

$$\sum_{k=1}^{m} N_k(x) f(x) = f(x), \quad x \in \Omega. \tag{3.4}$$

In Eq. (3.3), finite element shape functions $N_k(x)$ can be used as the local enrichment functions or the basic functions to produce a desired field within the domain Ω_{enr} [20]

$$f(x) = \sum_{i \in N_{enr}} N_i(x) f(x), \quad x \in \Omega_{enr}, \tag{3.5}$$

where N_{enr} denotes a set of crack surface and crack tip enriched nodes. Furthermore, the enrichment function $f(x)$ can be generalized to a set of n enrichment functions L that can represent crack tip analytic fields Ψ, i.e.,

$$L = (f_1, f_2, f_3, \cdots, f_n). \tag{3.6}$$

Hence, the crack tip field can be represented as

$$\Psi = \sum_{i \in N_{enr}} N_i \Big[\sum_n f_n(x) a_{in} \Big], \quad x \in \Omega_{enr}. \tag{3.7}$$

For conventional finite element nodes, the displacement field can be written as

$$u^{FEM} = \sum_{i \in I} N_i(x) u_i, \tag{3.8}$$

where I denotes all nodes in mesh; and u_i is conventional finite element node displacement. Fig. 2 (see [30]) shows the enriched nodes with fixing the near-tip enrichment scheme.

Fig. 3 illustrates the commonly-used topological enrichment strategy in XFEM. The circled nodes denote the generalized Heaviside function enriched nodes (N_{cr}), while the squared nodes denote the crack-tip enriched nodes (set N_{Tip}).

For the nodes around crack surface, the enrichment function can be generalized by Heaviside discontinuity enrichment function which is defined as

$$H(x) = \begin{cases} +1, & \text{above crack,} \\ -1, & \text{below crack,} \end{cases} \tag{3.9}$$

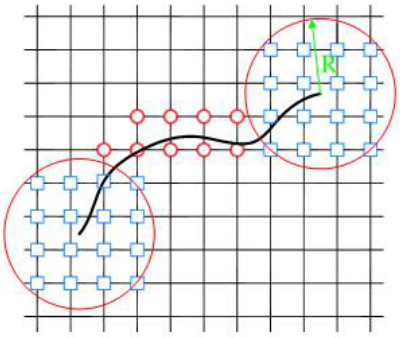

Figure 2: Fixing the near-tip enrichment (geometrical enrichment) scheme for selection of enriched nodes for 2D crack problem. Circled nodes(set of nodes N_{cr}) are enriched by the generalized Heaviside function, while squared nodes(set of nodes N_{Tip}) are enriched by the crack tip functions.

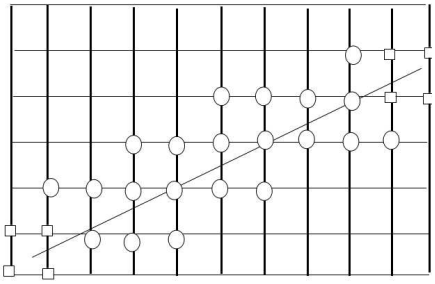

Figure 3: Topological enrichment in XFEM.

and then the Heaviside enrichment part of extended finite element displacement approximation can be written as

$$u^H = \sum_{n \in N_{cr}} N_n(x) H(x) a_n, \tag{3.10}$$

where N_{cr} denotes the Heaviside function enriched nodes (Circled nodes in Fig. 2); and a_n is the additional degree of freedom associated with the Heaviside enrichment. Hence, the Heaviside function enables modeling of a crack cutting a finite element.

For the nodes around crack tip (squared nodes in Fig. 2), the anisotropic crack tip enrichments [18] are applied to accurately reproduce the highly non-linear and singular stress and displacement fields.The displacement approximation around the crack tip can be expressed as follows:

$$u^{Tip} = \sum_{k \in N_{Tip}} N_k(x) \sum_{\alpha} F_\alpha(x) b_k^\alpha, \tag{3.11}$$

where N_{Tip} denotes the crack tip function enriched nodes (squared nodes in Fig. 2); F_α is

the crack tip enrichment function (described below); and b_k^α is the additional degree of freedom associated with the crack tip enrichment.

The crack tip enrichment functions can span the analytic asymptotic displacement fields around the crack tip (i.e., Eq. (2.1)). By expanding Eq. (2.1), we can get the asymptotic displacements fields [18]

$$u_1(r,\theta)=\sqrt{\frac{2r}{\pi}}\left[K_I(Re[A_{11}B_{11}^{-1}\beta_1+A_{12}B_{21}^{-1}\beta_2])+K_{II}(Re[A_{11}B_{12}^{-1}\beta_1+A_{22}B_{22}^{-1}\beta_2])\right], \tag{3.12a}$$

$$u_2(r,\theta)=\sqrt{\frac{2r}{\pi}}\left[K_I(Re[A_{21}B_{11}^{-1}\beta_1+A_{22}B_{21}^{-1}\beta_2])+K_{II}(Re[A_{21}B_{12}^{-1}\beta_1+A_{22}B_{22}^{-1}\beta_2])\right], \tag{3.12b}$$

where $\theta_i=\sqrt{\cos\theta+\mu_i\sin\theta}$; and μ_i represents the eigenvalues from Eq. (2.4). Thus, the anisotropic crack tip enrichment functions can be derived from Eqs. (3.12a) and (3.12b) as

$$F_\alpha(r,\theta)=\sqrt{r}\left\{\begin{array}{l} Re[A_{11}B_{11}^{-1}\beta_1+A_{12}B_{21}^{-1}\beta_2] \\ Re[A_{11}B_{12}^{-1}\beta_1+A_{12}B_{22}^{-1}\beta_2] \\ Re[A_{21}B_{11}^{-1}\beta_1+A_{22}B_{21}^{-1}\beta_2] \\ Re[A_{21}B_{12}^{-1}\beta_1+A_{22}B_{22}^{-1}\beta_2] \end{array}\right\}. \tag{3.13}$$

Eq. (3.13) can also be expressed in matrix form

$$F_\alpha(r,\theta)=\sqrt{r}\left\{Re\left[\frac{B^{-1}A_1\beta}{B^{-1}A_2\beta}\right]\right\}, \tag{3.14}$$

where

$$A_1=[A_{11}A_{12}],\quad A_2=[A_{21}A_{22}]\quad\text{and}\quad \beta=\left[\begin{array}{cc}\beta_1 & 0\\ 0 & \beta_2\end{array}\right].$$

In anisotropic medium, the matrices A and B depend on the properties of anisotropic materials, but are not related to the coordinate system.

For the thermal equation, the following tip enrichment proposed by Duflot [19] is adopted:

$$F^{th}(r,\theta)=\sqrt{r}\sin\left(\frac{\theta}{2}\right). \tag{3.15}$$

For mechanical problem, the displacement approximation can be written by using the standard FEM and the enriched XFEM

$$u^h=u^{FEM}+u^H+u^{Tip}. \tag{3.16}$$

Substituting Eqs. (3.8), (3.10) and (3.11) into Eq. (3.16), the XFEM displacement approximation can be obtained as

$$u^h=\sum_{i\in I}N_i(x)u_i+\sum_{n\in N_{cr}}N_n(x)H(x)a_n+\sum_{k\in N_{Tip}}N_k(x)\sum_\alpha F_\alpha(x)b_k^\alpha. \tag{3.17}$$

Similarly, for thermal problem, the XFEM temperature approximation can be written as

$$T^h=\sum_{i\in I}N_i(x)T_i+\sum_{n\in N_{cr}}N_n(x)H(x)c_n+\sum_{k\in N_{Tip}}N_k(x)F^{th}(x)d_k, \tag{3.18}$$

where T_i is finite element node temperature; c_n is the additional degree of freedom related to crack surface Heaviside enrichment; d_k is the additional degree of freedom related to crack tip enrichment; and F^{th} is the crack tip enrichment for temperature field, written as Eq. (3.15).

3.2.2 Thermoelastic XFEM discretization

For mechanical problem, the discretized form of the mechanical equation [22] can be gotten from Eq. (3.1g)

$$Ku^h=f, \tag{3.19}$$

where the approximation of displacement u^h is composed of usual and additional degrees of freedom:

$$u^h=(uab_1b_2b_3b_4). \tag{3.20}$$

The assembling of global stiffness matrix K and the mechanical force vectorcan follow the method of S. Mohammadi [23]

$$K_{ij}^e=\begin{bmatrix} K_{ij}^{uu}K_{ij}^{ua} & K_{ij}^{ub} \\ K_{ij}^{au}K_{ij}^{aa} & K_{ij}^{ab} \\ K_{ij}^{bu}K_{ij}^{ba} & K_{ij}^{bb} \end{bmatrix}, \tag{3.21a}$$

$$f_i=(f_i^u f_i^a f_i^{b_1} f_i^{b_2} f_i^{b_3} f_i^{b_4}), \tag{3.21b}$$

where

$$K^{rs}=\int_{\Omega_e}(B^r)^T CB^s d\Omega, \quad (r,s=u,a,b), \tag{3.22a}$$

$$f_i^u=\int_{\Gamma_t}N_i\bar{t}d\Gamma+\int_{\Omega_e}N_i\bar{b}d\Omega, \tag{3.22b}$$

$$f_i^a=\int_{\Gamma_t}N_iH\bar{t}d\Gamma+\int_{\Omega_e}N_iH\bar{b}d\Omega, \tag{3.22c}$$

$$f_i^b=\int_{\Gamma_t}N_iF_\alpha\bar{t}d\Gamma+\int_{\Omega_e}N_iF_\alpha\bar{b}d\Omega, \quad (\alpha=1,2,3,4), \tag{3.22d}$$

$$B_i^u = \begin{bmatrix} N_{i,x} & 0 \\ 0 & N_{i,y} \\ N_{i,y} & N_{i,x} \end{bmatrix}, \tag{3.22e}$$

$$B_i^a = \begin{bmatrix} (N_iH)_{,x} & 0 \\ 0 & (N_iH)_{,y} \\ (N_iH)_{,y} & (N_iH)_{,x} \end{bmatrix}, \tag{3.22f}$$

$$B_i^b = [B_i^{b_1} B_i^{b_2} B_i^{b_3} B_i^{b_4}], \tag{3.22g}$$

$$B_i^{b_\alpha} = \begin{bmatrix} (N_iF_\alpha)_{,x} & 0 \\ 0 & (N_iF_\alpha)_{,y} \\ (N_iF_\alpha)_{,y} & (N_iF_\alpha)_{,x} \end{bmatrix}, \quad (\alpha = 1,2,3,4). \tag{3.22h}$$

In Eqs. (3.22a)-(3.22h), $\bar{t}$ is the prescribed external traction on Γ_t; $\bar{b}$ is the body force; C is the anisotropic elastic matrix; F_α represents the anisotropic crack tip enrichment functions defined as Eq. (3.13); N_i represents the finite element shape functions; B represents the matrices of shape functions derivatives; and H represents the generalized Heaviside enrichment functions defined as Eq. (3.9).

For thermal problem, the discretized form of the thermal equation can be obtained from Eq. (3.1a)

$$MT^h + f^{th} = 0, \tag{3.23}$$

where the temperature approximation vector T^h is defined according to Eq. (3.20) as:

$$T^h = (Tcd). \tag{3.24}$$

Here, the meaning of c and d can refer to Eq. (3.18).

Assembling of the thermal stiffness matrix M and the thermal force vector f^{th} is similar to Eqs. (3.21a) and (3.21b), which can be written as below

$$M_{ij}^e = \begin{bmatrix} M_{ij}^{uu} M_{ij}^{ua} & M_{ij}^{ub} \\ M_{ij}^{au} M_{ij}^{aa} & M_{ij}^{ab} \\ M_{ij}^{bu} M_{ij}^{ba} & M_{ij}^{bb} \end{bmatrix}, \tag{3.25a}$$

$$f_i^{th} = (f_i^T f_i^c f_i^d)^T, \tag{3.25b}$$

where

$$M^{rs} = \int_{\Omega_e} (B_{th}^r)^T k B_{th}^s d\Omega, \quad (r,s = T,c,d), \tag{3.26a}$$

$$f_i^T = \int_{\Gamma_q} N_i \bar{q} d\Gamma, \tag{3.26b}$$

$$f_i^c = \int_{\Gamma_q} N_i H \bar{q} d\Gamma, \tag{3.26c}$$

$$f_i^d = \int_{\Gamma_q} N_i F^{th} \bar{q} d\Gamma, \tag{3.26d}$$

$$B^u_{ith}=\begin{bmatrix} N_{i,x} \\ N_{i,y} \end{bmatrix}, \tag{3.26e}$$

$$B^c_{ith}=\begin{bmatrix} (N_iH)_{,x} \\ (N_iH)_{,y} \end{bmatrix}, \tag{3.26f}$$

$$B^d_{ith}=\begin{bmatrix} (N_iF^{th})_{,x} \\ (N_iF^{th})_{,y} \end{bmatrix}. \tag{3.26g}$$

In Eqs. (3.26b)-(3.26g), F^{th} represents the crack tip enrichment function for thermal equation, which is defined as Eq. (3.15); and k is the matrix of heat conductivity, which is defined as Eq. (3.1a).

After solving the thermal equation of Eq. (3.23), the thermal strain ε_T can be calculated from Eq. (3.1d). Thus, the global force vector can be written as

$$f=f^{th}+f^{mech}=\int_\Omega B^T C\varepsilon^T d\Omega+f^{mech}, \tag{3.27}$$

where B is defined as Eqs. (3.22e)-(3.22h).

4 Evaluation of SIFs using interaction integral method

In this study, the domain formulation of interaction integral for thermal problem [17, 18, 24, 25] is adopted to solve the SIFs.

$$J=\lim_{\Gamma\to 0}\int_\Gamma (W\delta_{1j}-\sigma_{ij}u_{i,1})n_j d\Gamma, \tag{4.1}$$

where i,j=1,2 denotes the two-dimensional problem; Γ is an arbitrary closed contour surrounding the crack-tip, as depicted in Fig. 3, n_j is the jth component of the outward unit vector normal to Γ; W is the strain energy density for thermoelastic anisotropic material, which is defined as

$$W=\frac{1}{2}\sigma_{ij}[\varepsilon_{ij}-\alpha_{ij}\Delta T], \tag{4.2}$$

and the constitutive equation is defined as

$$\sigma_{ij}=C_{ijkl}[\varepsilon_{kl}-\alpha_{kl}\Delta T], \tag{4.3}$$

in which C_{ijkl} represents the components of anisotropic constitutive tensor, α_{kl} represents the components of thermal expansion coefficient vector, and ΔT represents the temperature difference from reference temperature.

Firstly, a weight function q is defined as an arbitrary function varying from unity at the crack tip to zero on Γ. Then, the divergence theorem is applied to Eq. (4.1), and thus the equivalent domain form can be given by

$$J=\int_A(\sigma_{ij}u_{i,1}-W\delta_{1j})q_{,j}dA+\int_A(\sigma_{ij}u_{i,1}-W\delta_{1j})_{,j}qdA, \tag{4.4}$$

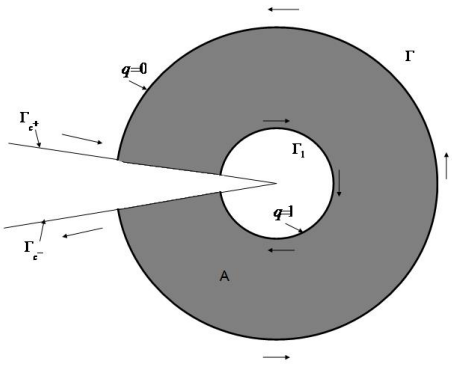

Figure 4: Area for domain integral (cited from [7]).

where A is the domain enclosed by Γ.

For homogeneous anisotropic materials, Eq. (4.4) can be recast into the domain form of thermal J-integral

$$J=\int_A(\sigma_{ij}u_{i,1}-W\delta_{1j})q_{,j}dA+\int_A(\sigma_{ij}\alpha_{ij}T_{,1})qdA. \tag{4.5}$$

Now, consider two states: a true one denoted as state (1), and an auxiliary one denoted as state (2). Here, the crack-tip asymptotic field is adopted as the auxiliary state (2). According to the generalized Stroh's formalism [27,28], it can also be expressed as Eqs. (2.2) and (2.3).

By superposing the true and auxiliary states, the J-integral can be written as

$$J^{(1+2)}=J^{(1)}+J^{(2)}+M^{(1,2)}, \tag{4.6}$$

where $M^{(1,2)}$ is the interaction integral. $M^{(1,2)}$ can be expressed as

$$M^{(1,2)}=\int_A(\sigma_{ij}^{(1)}u_{i,1}^{(2)}+\sigma_{ij}^{(2)}u_{i,1}^{(1)})-\frac{1}{2}(\sigma_{ij}^{(1)}\varepsilon_{ij}^{(2)}+\sigma_{ij}^{(2)}\varepsilon_{ij}^{*})\delta_{1j}q_{,j}dA+\int_A(\sigma_{ij}^{(2)}\alpha_{ij}^{(1)}T_{,1}^{(1)})qdA, \tag{4.7}$$

where $\varepsilon_{ij}^{*}=\varepsilon_{ij}^{(1)}-\alpha_{ij}^{(1)}(\Delta T)^1$, and superscripts 1, 2 and 1+2 respectively denote the fields and quantities related to states 1, 2 and 1+2.

For elastic anisotropic solids under mixed-mode loading, the J-integral is associated with both the energy release rate and the SIFs as [3]

$$J=\frac{1}{2}KLK^T, \tag{4.8}$$

where $K=[K_IK_{II}]$ is the mixed-mode SIFs; and L is a 2×2 Irwin matrix that is dependent on the anisotropic material properties as below:

$$L=Re(i\cdot AB^{-1})\Delta, \tag{4.9}$$

where *Re* denotes real part, and the details of matrices A and B can refer to [18].

Therefore, for 2D problem, the relation between SIFs and J-integral can be written as

$$J=\frac{1}{2}K_{II}^2L_{11}+\frac{1}{2}K_I^2L_{22}+K_IK_{II}L_{12}. \tag{4.10}$$

Substituting Eq. (4.10) into Eq. (4.5), the formulation of interaction integral $M^{(1,2)}$ can be rewritten as

$$M^{(1,2)}=K_{II}^{(1)}K_{II}^{(2)}L_{11}+K_I^{(1)}K_I^{(2)}L_{22}+(K_I^{(1)}K_{II}^{(2)}+K_{II}^{(1)}K_I^{(2)})L_{12}. \tag{4.11}$$

Assuming $K_I^{(2)}=1$ and $K_{II}^{(2)}=0$, then Eq. (4.11) reduces to

$$M^{(1,I)}=K_I^{(1)}L_{22}+K_{II}^{(1)}L_{12}. \tag{4.12}$$

Assuming $K_I^{(2)}=0$ and $K_{II}^{(2)}=1$, then Eq. (4.11) reduces to

$$M^{(1,II)}=K_{II}^{(1)}L_{11}+K_I^{(1)}L_{12}. \tag{4.13}$$

Therefore, the mixed-mode SIFs, i.e., $K_I^{(1)}$ and $K_{II}^{(1)}$, can be obtained by solving a system of linear algebraic Eqs. (4.12) and (4.13).

5 Numerical simulations

In order to demonstrate the effectiveness and accuracy of the proposed method, several numerical examples are evaluated in this section and the obtained SIFs are compared with available numerical reference solutions. To be specific, different material properties, crack-tip enrichments schemes, the radius of J-integral and the density of mesh are considered to show the effects of these parameters on the anisotropic SIFs.

Due to the presence of enrichment term in XFEM, the quadrature requires different Gauss quadrature in different elements. Therefore, the sub domain integration is adopted here, as depicted in Fig. 5 (see [20]). Here, a 2×2 Gaussian quadrature is applied to unenriched elements, a 3×3 Gaussian quadrature is used in sub-triangles containing Heaviside function enriched node(s), and a 5×5 Gaussian quadrature is applied to sub-triangles containing crack tip function enriched node(s).

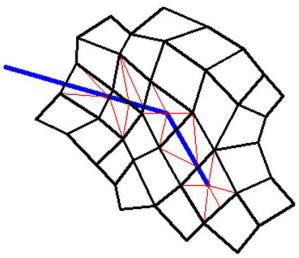

Figure 5: Integration sub domain in XFEM.

5.1 Infinite plate with an inclined insulated crack

An inclined insulated crack in the plane stress condition is considered to compare the SIFs calculated from those of boundary element method [12].

As depicted in Fig. 6, a crack with a length of $2a$ and an angle of γ to x axis exists in an infinite medium. Here, in order to simulate the infinity of the medium, the length and width of plate are both set to $40a$, and the steady and uniform heat at infinity, h^{∞}, is flowing in the direction of y axis.

The material is anisotropic glass/epoxy [13], and its material properties are: $E_{11}=55\text{GPa}$, $E_{22}=21\text{GPa}$, $\nu_{12}=0.25$, $G_{12}=9.7\text{GPa}$, $\alpha_1=6.3\times10^{-6}\text{K}^{-1}$, $\alpha_2=2\times10^{-5}\text{K}^{-1}$, $k_1/k_2=3.46/0.35$.

A finite element mesh with 1600 quadrilateral elements and 1681 nodes is employed for fracture analysis by XFEM. The radius of J-integral is $1.5a$, and the enriched nodes around crack tip are marked by red hexagram, as shown in Fig. 7.

Table 1 gives the SIFs at the left tip of the crack with variation of inclination angles γ

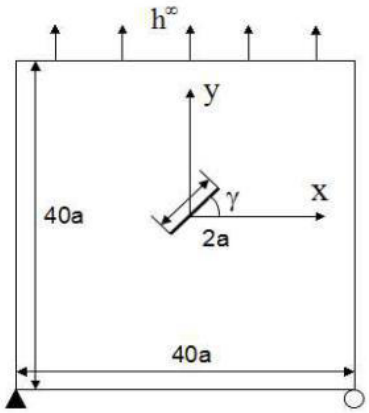

Figure 6: Infinite plate with an inclined insulated crack under steady and uniform heat flux at infinity.

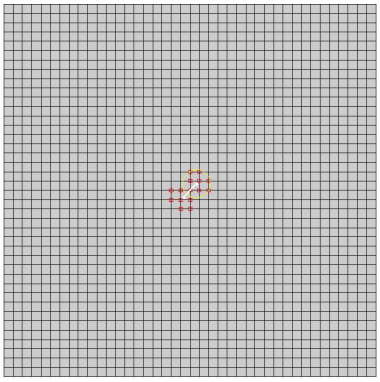

Figure 7: XFEM mesh for Example 1 (the red hexagram denotes crack tip function enriched nodes).

Table 1: The SIFs of the inclined insulated crack.

crack angle (degree)	$\frac{K_I}{K_0}$ exact [29]	$\frac{K_I}{K_0}$ [12]	$\frac{K_I}{K_0}$ present	$\frac{K_{II}}{K_0}$ exact [29]	$\frac{K_{II}}{K_0}$ [12]	$\frac{K_{II}}{K_0}$ present
0	0.0000	0.0000	0.0000	0.3657	0.3664	0.3660
30	0.3279	0.3284	0.3282	0.5060	0.5069	0.5068
45	0.3091	0.3097	0.3095	0.5677	0.5687	0.5679
60	0.1893	0.1896	0.1905	0.5107	0.5116	0.5113
75	0.0566	0.0567	0.0569	0.3058	0.3063	0.3069

in comparison with those obtained by BEM [12] and analytical solution [29].

$$K_0 = \frac{a\sqrt{\pi a}E_{11}\alpha_1 h^{\infty}}{k_1}$$

is adopted to normalize the SIFs. As can be seen from Table 1, the numerical results of the present XFEM agree well with those obtained by BEM or analytical method, and the relative error does not exceed 0.3%.

5.2 Inclined central crack under temperature field

The second example is a rectangular plate with an insulated central crack, which was previously studied by Y. C. Shiah and C. L. Tan [13]. As shown in Fig. 8, its length is $4W$, its width is W, the inclined angle of the crack is γ, and the two ends of the plate (AB and CD) are constrained in the y direction but free to x direction.

The plate is subjected to a uniform temperature field load. The central crack surfaces and the two sides of BC and AD are all thermally insulated. The side of AB is maintained at its original temperature, but the side of CD is cooled by temperature Θ_0 The material medium of the plate is glass/epoxy [13].

In this example, three values of γ are chosen: 0°, 30° and 45°. The SIFs are computed for relative crack lengths, a/W of $0.1 \sim 0.5$. The computed SIFs are normalized by $K_0 = \sqrt{\pi a}E^*_{22}\alpha^*_2\Theta_0$.

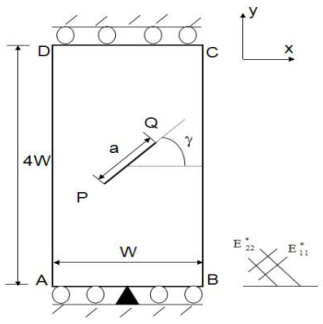

Figure 8: Inclined central crack.

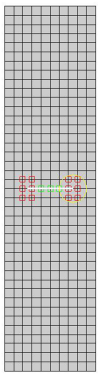

Figure 9: FEM mesh for inclined central crack with the relative radius of J-integral $r/a=0.3$ (the red square nodes are crack tip function enriched nodes, while the green square nodes are Heaviside function enriched nodes).

Fig. 9 shows the FEM mesh used to solve the thermal problem and mechanical problem. The mesh contains 451 nodes and 400 4-noded quadrilateral elements for $a/W=0.5$ and $\gamma=0^\circ$. The relative radius of J-integral r/a is 0.3.

The simulated results of the normalised SIFs for the crack-tip Q are given in Table 2. As can be seen, the normalized SIFs obtained using the proposed thermoelastic XFEM agree excellently with those obtained using BEM [13], and the percent difference is no less than 4.4.

Fig. 10 demonstrates the effects of mesh refinement on the normalized SIFs at the crack-tip Q in the case of $\gamma=30^\circ$ for $a/W=0.5$, using both topological and geometrical (fixed near-tip) crack tip enrichment schemes. Five different mesh refinements are used

Table 2: Normalized SIFs for the crack-tip Q.

γ (degree)	a/W	[13] ($\frac{K_I}{K_0}$)	present ($\frac{K_I}{K_0}$)	% Diff	[13] ($\frac{K_{II}}{K_0}$)	present ($\frac{K_{II}}{K_0}$)	% Diff
0	0.1	0.361	0.366	1.2	0.000	0.000	-
	0.2	0.371	0.373	0.5	0.000	0.000	-
	0.3	0.367	0.367	0.0	0.001	0.001	-
	0.4	0.372	0.376	1.0	0.002	0.002	-
	0.5	0.381	0.384	0.8	0.002	0.002	-
30	0.1	0.269	0.274	1.2	0.159	0.161	1.5
	0.2	0.274	0.276	0.4	0.157	0.151	3.1
	0.3	0.281	0.281	0.0	0.155	0.150	3.1
	0.4	0.290	0.295	1.2	0.152	0.152	0.0
	0.5	0.303	0.303	0.0	0.149	0.153	4.4
45	0.1	0.147	0.148	0.4	0.195	0.187	3.9
	0.2	0.196	0.193	0.8	0.174	0.168	3.1
	0.3	0.208	0.215	1.4	0.174	0.169	3.0
	0.4	0.224	0.221	0.8	0.174	0.166	3.8
	0.5	0.188	0.191	0.6	0.186	0.182	2.0

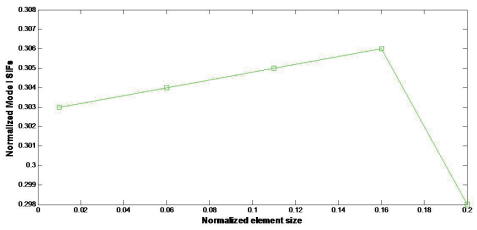

(a) Convergence of the $\frac{K_I}{K_0}$ in case of $\gamma=30^\circ$ using topological enrichment scheme

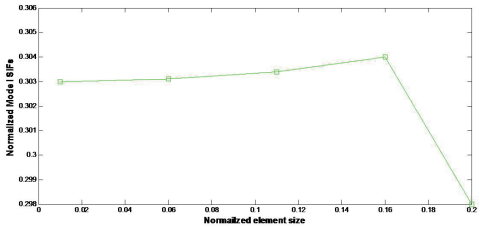

(b) Convergence of the $\frac{K_I}{K_0}$ in case of $\gamma=30^\circ$ using geometry enrichment scheme

Figure 10: Convergence of the $\frac{K_I}{K_0}$ using topological enrichment scheme.

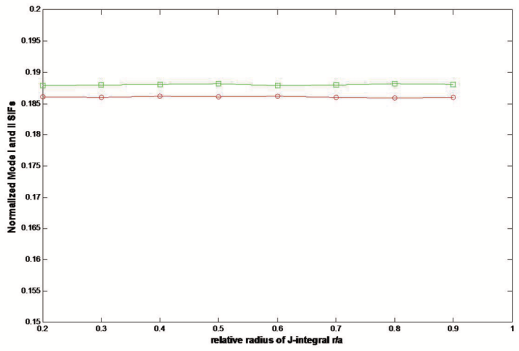

Figure 11: Path-independent J-integral.

with a normalized characteristic element length h/W varying between 0.01 and 0.2.

Fig. 10(a) shows the convergence of the $\frac{K_I}{K_0}$ in the case of $\gamma=30^\circ$ using topological enrichment scheme, while Fig. 10(b) shows the convergence of the $\frac{K_I}{K_0}$ in the case of $\gamma=30^\circ$ using fixed near-tip enrichment domain scheme. From Fig. 10, it can be seen that most of the results are within 0.6%, and that the geometry enrichment scheme can improve the convergence of SIFs significantly.

Fig. 11 depicts the normalized SIFs ($\frac{K_I}{K_0}$ and $\frac{K_{II}}{K_0}$) obtained from different relative radii of J-integral r/a for the case of $\gamma=45^\circ$ and $a/W=0.5$. It is found from this figure that the J-integral is practically path-independent.

5.3 Two parallel cracks

In this example, an anisotropic square plate with two parallel cracks is studied. As depicted in Fig. 12, the length and width of the plate are $2L$ and $2L$, respectively; the lengths of crack are both equal to a; and the distance between the two cracks is $2d$. Here, five relative crack lengths ($a/L=0.1,0.2,0.3,0.4,0.5$) and two relative distance values between the two cracks ($d/L=0.1,0.3$) are considered.

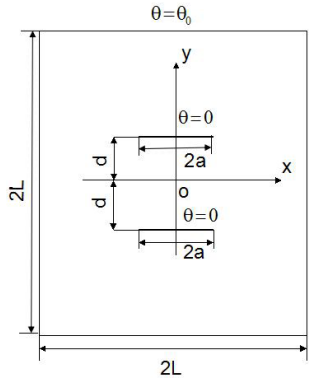

Figure 12: Two parallel cracks.

Table 3: Comparison of the computed SIFs and those from [12]at the right tip of the bottom crack.

a/L	[12] (d/L:0.1)	present (d/L:0.1)	[12] (d/L:0.2)	present (d/L:0.2)	[12] (d/L:0.3)	present (d/L:0.3)
0.1	0.175	0.176	0.183	0.181	0.170	0.171
0.2	0.153	0.154	0.164	0.165	0.157	0.158
0.3	0.142	0.141	0.153	0.153	0.147	0.146
0.4	0.135	0.136	0.146	0.146	0.139	0.138
0.5	0.130	0.128	0.137	0.136	0.133	0.131

The plate material is glass/epoxy [12]. The temperature of crack faces is fixed at zero degree, and the boundaries of the plate are heated by the temperature θ_0 The mechanical boundary conditions are on the two crack faces and the boundaries of the plate, and the traction are free. According to the thermal condition, the Mode I SIF dominates while the computed Mode II SIF is very small, so that the Mode II SIFs are neglected here.

Table 3 gives the computed SIFs and those obtained from BEM [12] at the right tip of the bottom crack, considering different crack lengths and distances between the two cracks. Here, all SIFs are normalized by the factor$K_0 = \sqrt{\pi a} E_{22} \alpha_2 \theta_0$

From Table 3, the results obtained by the two methods are very close, which can confirm the accuracy of the proposed method. Besides, it can also be found that the $\frac{K_I}{K_0}$ decreases with the increase of relative crack length a/L. For longer cracks, the distance between them has no influence on the Mode I SIFs; for the same crack relative length, the monotonous dependence of Mode I SIFs on the relative distance d/L between cracks is not observed.

6 Conclusions

In summary, XFEM with Stroh's formalism of crack tip enrichment functions was firstly applied to the simulation of generally anisotropic thermoelastic fracture problems. The thermal form of interaction energy integral was adopted to extract the thermomechanical SIFs, and numerical examples were given to justify the validity of the proposed method.

In addition, the presented method can also be applied to curved thermomechanical fracture problems in generally anisotropic materials, which can be viewed as its another advantage.

Acknowledgments

This work was supported by the National Natural Science Foundation of China (No. 11471262).

References

[1] N. I. MUSKHELISHVILI, Some Basic Problems of the Mathematical Theory of Elasticity, 2nd edn, Noordhoff, Leiden, 1953.
[2] G. C. SIH, P. PARIS AND G. IRWIN, *On cracks in rectilinearly anisotropic bodies,* Int. J. Fract. Mech., 1 (1965), pp. 189–203.
[3] Z. SUO, *Singularities, interfaces and cracks in dissimilar anisotropic media,* Proc. R. Soc. Lond. A, 427 (1990), pp. 331–358.
[4] L. NOBILE AND C. CARLONI, *Fracture analysis for orthotropic cracked plates,* Compos. Struct, 68 (2005), pp. 285–293.
[5] S. G. LEKHNITSKII, Theory of Elasticity of an Anisotropic Elastic Body, Science Press, Beijing, 1963.
[6] S. Q. ZHANG AND W. Y. YANG, *Prediction of mode I crack propagation direction in carbon-fiber reinforced composite plate,* Appl. Math. Mech., 25 (2004), pp. 714–721.
[7] H. G. JIA, Y. F. NIE AND J. L. LI, *Fracture analysis in orthotropic thermoelasticity using extended finite element method,* Adv. Appl. Math. Mech., 7 (2015), pp. 780–795.
[8] J. H. CHANG AND G. J. LIAO, *Nonhomogenized displacement discontinuity dethod for calculation of stree intensity factors for cracks in anisotropic FGMs,* J. Eng. Mech., 140 (2014).
[9] F. K. CETISLI AND O. METE, *Numerical analysis of interface crack prooblem in composite plates jointed with composite patch,* Steel. Compos. Struct., 16 (2014), pp. 203–220.
[10] N. N. V. PRASAD, M. H. ALIABADI AND D. P. ROOKE, *The dual boundary element method for thermoelastic crack problems,* Int. J. Fract., 47 (2009), pp. 1926–1938.
[11] A. TAFRESHI, *Fracture mechanics analysis of composite structures using the boundary element shape sensitivities,* AIAA. J., 23 (1999), pp. 87–96.
[12] I. PASTERNAK, *Boundary integral equations and the boundary element method for fracture mechanics analysis in 2D anisotropic thermoelasticity,* Eng. Anal. Bound. Elem., 36 (2012), pp. 1931–1941.
[13] Y. C. SHIAH AND C. L. TAN, *Fracture mechanics analysis in 2-D anisotropic thermoelasticity using BEM,* Comp. Model. Eng., 3 (2000), pp. 91–99.
[14] K. N. RAJESH AND B. N. RAO, *Two-dimensional analysis of anisotropic crack problems using coupled meshless and fractal finite element method,* Int. J. Fract., 164 (2010), pp. 285–318.
[15] J. BELINHA AND L. M. J. S. DINIS, *Nonlinear analysis of plates and laminates using the element free Galerkin method,* Compos. Struct., 78 (2007), pp. 337–350.
[16] L. BOUHALA, A. MAKRADI AND S. BELOUETTAR, *Thermal and thermo-mechanical influence on crack propagation using an extended mesh free method,* Eng. Fract. Mech., 88 (2012), pp. 35–48.

[17] A. ASADPOURE AND S. MOHAMMADI, *Developing new enrichment functions for crack simulation in orthotropic media by the extended finite element method,* Int. J. Numer. Meth. Eng., 69 (2007), pp. 2150–2172.
[18] G. HATTORI, R. ROJAS-DÍAZ, A. SÁEZ, N. SUKUMAR AND F. GARCÍA-SÁNCHEZ, *New anisotropic crack-tip enrichment functions for the extended finite element method,* Comput. Mech., 50 (2012), pp. 591–601.
[19] M. DUFLOT, *The extended finite element method in thermoelastic fracture mechanics,* Int. J. Numer. Meth. Eng., 74 (2008), pp. 827–847.
[20] S. HOSSEINI, H. BAYESTEH AND S. MOHAMMADI, *Thermo-mechanical xfem crack propagation analysis of functionally graded materials,* Math. Sci. Eng. A, 561 (2013), pp. 285–302.
[21] U. OZKAN, H. F. NIED AND A. C. KAYA, *Fracture analysis of anisotropic materials using enriched crack tip elements,* Eng. Fract. Mech., 77 (2010), pp. 1191–1202.
[22] H. BAYESTEH, A. AFSHAR AND S. MOHAMMADI, *Thermo-mechanical fracture study of inhomogeneous cracked solids by the extended isogeometric analysis method,* Euro. J. Mech. A-Solid, 51 (2015), pp. 123–139.
[23] S. MOHAMMADI, Extended Finite Element Method for Fracture Analysis of Structures, Blackwell, UK, 2008.
[24] J. CHEN, *Determination of thermal stress intensity factors for an interface crack in a graded orthotropic coating substrate structure,* Int. J. Fract., 133 (2005), pp. 302–328.
[25] N. MOËS, J. DOLBOW AND T. BELYTSCHKO, *A finite element method for crack growth without remeshing,* Int. J. Numer. Meth. Eng., 46 (1999), pp. 131–150.
[26] J. R. RICE, *A path independent integral and the approximate analysis of strain concentration by notches and cracks,* J. Appl. Mech., 35 (1968), pp. 379–386.
[27] A. STROH, *Dislocation and cracks in anisotrpic elasticity*, Philos. Mag., 3 (1958), pp. 625–646.
[28] T. C. T. TING, Anisotropic Elasticity, Oxford University Press, New York, 1996.
[29] C. HWU, Anisotropic Elastic Plates, Springer, London, 2010.
[30] S. BORDAS, P. V. NGUYEN, C. DUNANT, A. GUIDOUM AND H. NGUYEN-DANG, *An extended finite element library,* Int. J. Numer. Meth. Eng., 71 (2007), pp. 703–732.